CSIRO PUBLISHING

www.publish.csiro.au/journals/ijwf *International Journal of Wildland Fire*, 2003, **12**, 259–270

Remote sensing of burned areas in tropical savannas

José M. C. Pereira

Cartography Centre, Tropical Research Institute, Travessa Conde da Ribeira 9, 1300-142 Lisboa, Portugal. Tel/Fax: 00351 21 364 0046; email: jmcpereira@isa.utl.pt

Abstract. Problematic aspects of fire in tropical savannas are reviewed, from the standpoint of their impact on the detection and mapping of burned areas using remotely sensed data. Those aspects include: the heterogeneity of savanna—resulting in heterogeneity of fire-induced spectral changes; fine fuels and low fuel loadings—resulting in short persistence of the char residue signal; tropical cloudiness—which makes multitemporal image compositing important; the frequent presence of extensive smoke aerosol layers during the fire season—which may obscure fire signals; and the potential problem of detecting burns in the understory of woody savannas with widely variable tree stand density, canopy cover and leaf area index. Finally, the capabilities and limitations of major satellite remote sensing systems for pan-tropical burned area mapping are addressed, considering the spatial, spectral, temporal and radiometric characteristics of the instruments.

Additional keywords: burned areas; fire; mapping.

Introduction

Savannas are tropical vegetation types in which the biomass is shared by trees and grass (van Wilgen and Scholes 1997), and have at least a two-layered above-ground structure, formed by a tree layer with a discontinuous crown cover 2–10 m tall, and an understory grass layer 0.5–2 m tall (Scholes 1997). Savannas are typical of the seasonally wet tropics (van Wilgen and Scholes 1997), which have a hot, wet season lasting between 4 and 8 months, and a dry season during the rest of the year. The strongly seasonal character of water availability leads to the accumulation of fine, dry, easily ignited fuels that, potentially, can burn every year (Scholes 1997). Estimates of annual global biomass burning indicate that savanna fires are the single largest source of pyrogenic emissions, with an area of $\sim 820 \times 10^6$ ha burned annually, and a corresponding consumption of 3400–3700 Tg of dry matter (Andreae 1997).

Dwyer *et al*. (2000) analysed 21 months (April 1992 to December 1993) of global, daytime, daily National Oceanic and Atmospheric Administration (NOAA)–Advanced Very High Resolution Radiometer (AVHRR) satellite data at 1 km resolution, and detected active fires using the algorithm of Flasse and Ceccato (1996). Savannas and woody savannas which, as defined in the International Geosphere-Biosphere Program–Data and Information System (IGBP-DIS) land cover map (Scepan 1999), represent ~11% of the global land surface, showed the most fire activity of all major land cover types. Active fires were detected in 19% of 1 km^2 savanna pixels during the period under analysis. The daily, global night-time, 1 km^2 resolution Along Track Scanning Radiometer (ATSR-2) active fires dataset (http://shark1.esrin.esa.it/ionia/FIRE/AF/ATSR/) developed by the European Space Agency (Fig. 1) contains a total of 525 488 active fire detections, over the period 1997–2001. Twenty-five percent of these (131 161 active fires) were found over the area of savanna and woody savanna classes of the IGBP-DIS land cover map located in the intertropical belt (23°27′N to 23°27′S), which corresponds to only 8.5% of the global land area (Mota and Pereira, unpublished work). These satellite-based observations of fire activity over the tropical savannas confirm them as the most fire-prone biome on Earth.

Active fires detected by satellite provide a good indicator of the spatio-temporal patterns of global fire incidence, but are inadequate to estimate area burned, mainly due to temporal sampling problems (Pereira *et al*. 1999*a*; Dwyer *et al*. 2000). Area burned is required to estimate pyrogenic emissions and fire return intervals, which are important parameters to estimate the impacts of fire on the atmosphere and on terrestrial ecosystems, respectively. Therefore, a series of studies have been developed to map area burned from satellite imagery, many of them dealing with tropical regions (Hlavka *et al*. 1995; Eva and Lambin 1998*a*, 1998*b*; Barbosa *et al*. 1999*a*, 1999*b*; Pereira *et al*. 1999*a*, 2000; Roy *et al*. 1999; Siegert and Hoffmann 2000; Stroppiana *et al*. 2002). Remote sensing of fire severity and fire patchiness, although important to quantify the ecological and atmospheric impacts of fire, is at an early stage of development (Rogan and Yool 2001; Miller and Yool 2002).

 10.1071/WF03028 1049-8001/03/030259

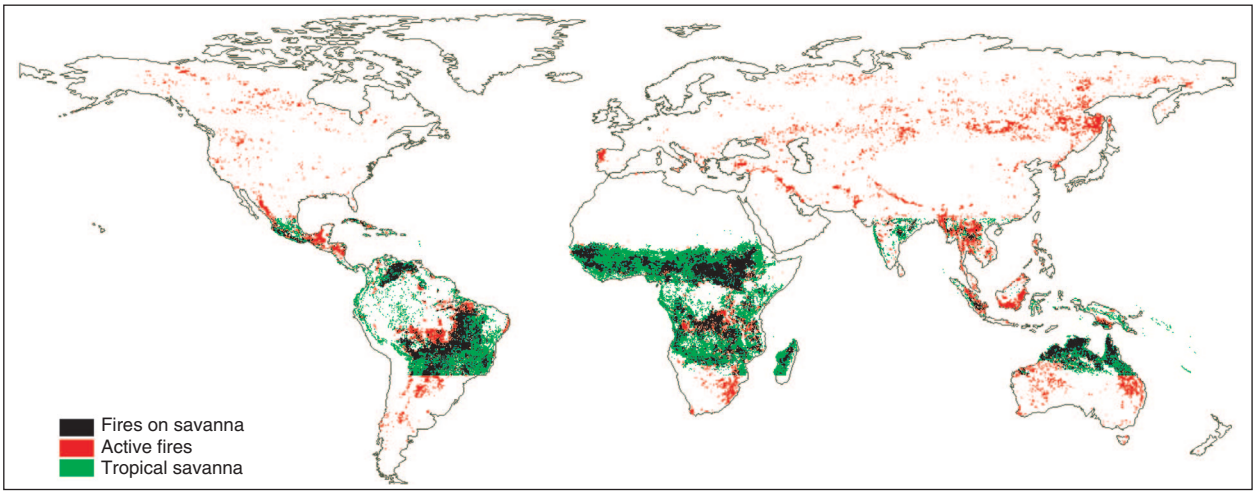

Fig. 1. Incidence of night-time active fires on tropical savannas, as detected by the European Remote Sensing (ERS-2) Along Track Scanning Radiometer (ATSR). The original data, at 1 km spatial resolution, were binned to 0.25° grid cells. Only those cells where a total of at least five active fires were detected during the 1997–2000 fire seasons were detected are represented. The 'tropical savanna', and 'fires on savanna' are bound by the Tropic of Cancer and Tropic of Capricorn, in the northern and southern hemispheres, respectively.

Our overview of remote sensing of fires in tropical savannas focuses on detection and mapping of area burned. The other types of signal generated by fires that can be observed from space, i.e. heat and light from active fire fronts, smoke, and modified vegetation structure (Robinson 1991), are addressed only when relevant to remote sensing of area burned. The overview is organised around key aspects of vegetation structure, fire regime features and climatic aspects of the savanna biome which influence detection and mapping of burned areas using satellite imagery.

Spectral changes induced by fire in tropical savannas

Savannas form a continuum of vegetation types between tropical forests and grasslands (House and Hall 2001) where tree percentage cover may range from 5% to 90% (Scholes 1997). Functional types of savanna trees include evergreen, semi-deciduous, and deciduous species (Scholes *et al*. 1997), the latter being more common in arid areas because leaf shedding reduces water stress (House and Hall 2001). The combination of canopy density and phenological strategy determine the amount of green foliage present in trees during the dry season. In humid savannas, tree cover is dense and relatively high tree leaf area index values are maintained throughout the dry season and thus the spectral signal of green vegetation is always present. Conversely, in drier areas, lower tree cover and more marked drought-deciduousness of trees lead to predominance of the spectral signal of dry grass and tree leaf litter during the fire season.

Savanna fires typically burn surface fuels, primarily grass and tree litter (van Wilgen and Scholes 1997), leaving a dark, charred surface. Figure 2 shows the spectral signatures of a deciduous tree leaf, dry grass, and charcoal, from 0.4 μm to 2.5 μm. The grass spectra were measured in the laboratory at

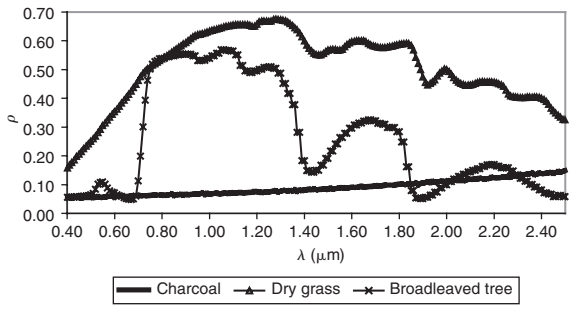

Fig. 2. Spectral signatures of pure charcoal fragments from a vegetation fire, dry grass, and a leaf from a broadleaved tree (0.4–2.5 μm). The vegetation signatures are from the Advanced Spaceborne Thermal Emission and Reflection Radiometer (ASTER) spectral reflectance signatures library (http://speclib.jpl.nasa.gov/). The charcoal signature was collected at the Jet Propulsion Laboratory, NASA, from samples supplied by the author.

Johns Hopkins University with a GER IRIS Mark IV spectroradiometer, using a large piece of sod. The grass was illuminated from directly above and measured at a reflectance angle of 60° to avoid viewing the thatch. The charcoal spectrum was obtained at the NASA Jet Propulsion Laboratory with a Beckman UV5240 spectrophotometer, from samples of charred pine stumps from a forest fire in central Portugal. The reflectance of charcoal and of green vegetation is similar in the visible domain, and to a lesser extent also in the mid-infrared. The reflectance of dry grass is much higher than that of charcoal over the entire spectral range. Thus, when burning occurs in the understory of relatively dense tree cover, the major reflectance change is a decrease in the near-infrared, while burning of dry grass under sparse tree cover or in open grasslands causes an overall decrease in reflectance.

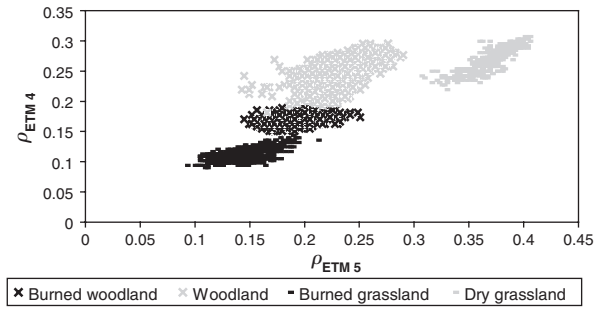

Fig. 3. Fire-induced spectral reflectance changes in a mid-infrared (ρ_{ETM5}, 1.65 μm) *v*. near-infrared (ρ_{ETM4}, 0.86 μm) bispectral space. Data from a Landsat 7 Enhanced Thematic Mapper scene from the Western Province, Zambia, dated September 2000.

Figure 3 displays the spectral changes due to surface charring in two southern African vegetation types, in a near-infrared (NIR, 0.87 μm)/mid-infrared (MIR, 1.65 μm) bispectral space, using Landsat 7 Enhanced Thematic Mapper (ETM+) data from western Zambia. Burning of woodland understory caused a decrease in NIR reflectance, but little change in MIR reflectance, while burning of a grassland caused a marked drop in reflectance along both spectral axes. The variability of the spectral changes induced by fire in tropical savannas is a direct consequence of the structural and phenological diversity of this biome, and variation in severity of fire effects, namely the degree of canopy scorch and consequent leaf fall. This variability ought to be taken into account in the design of algorithms for burned area mapping. Other fire-prone biomes, such as boreal forests, temperate shrublands, tropical grasslands, and temperate grasslands are less structurally and/or phenologically diverse. In forests and shrublands, fires burn primarily green fuels, while in grasslands dry vegetation is the dominant fuel type, and thus there is clear predominance of either one of the two types of spectral changes observable in savannas.

The heterogeneity of spectral changes caused by fire needs to be taken into account in satellite image classification, because the informational class (*sensu* Swain 1978) 'burned surface' may correspond to multiple spectral classes. In an unsupervised classification approach, burned surfaces may correspond to more than one spectral cluster. In supervised image classification it may be necessary to train the classifier to recognize different classes of burned areas, each of which ought to have a reasonable degree of internal spectral homogeneity and as little overlap as possible with other informational classes. In this regard, methods such as classification trees (Breiman *et al*. 1984; Mitchell 1997) are advantageous, because they can be trained with a single fire class. The statistical algorithm will identify internal spectral class heterogeneity and will induce different rules to classify the various spectral subsets corresponding to the single 'burned areas' informational class it was trained to recognize. Applications of classification trees to mapping burned areas with satellite imagery were developed by Pereira *et al*. (1999*b*, 2000) and Sá *et al*. (2003*a*). Spectral heterogeneity of the burn signal also influences the performance of adaptive, context-sensitive algorithms (Roy *et al*. 2002).

Biomass burned and persistence of the char signal

The biomass burnt per unit area in tropical savannas tends to be lower than that consumed in temperate and boreal forest and shrubland fires (Bond and van Wilgen 1996). Table 1 summarizes biomass and combustion completeness data from tropical savanna fire experiments in Brazil, Africa and Australia. The median pre-fire biomass load is 5.6 t ha^{-1}, the median combustion completeness is 0.81, and the median biomass consumed is 3.1 t ha^{-1}. The sample of experiments shown in Table 1 is not meant to be statistically representative of biomass burning in tropical savannas, but provides an indication of the range of values observed in different continents and various ecosystems.

Fuel consumption values of 6.1–16.1 t ha^{-1} were reported by Fernandes *et al*. (2000) for shrublands in Portugal, and calculations based on values from Keith *et al*. (2002) yield values of 8.4–18.7 t ha^{-1} in Australian heathlands, assuming a fuel heat content of 20 000 kJ kg^{-1}. The mean value of fuel burned in boreal forest fires in nine ecozones in Alaska was 17.4 t ha^{-1} (French *et al*. 2000), and a high intensity experimental forest fire in Siberia burned 37.1 t ha^{-1} (FIRESCAN Science Team 1996). Ward (2001) considered an average fuel consumption of 45 t ha^{-1} for forest fires in the United States.

The type of fuel burnt also differs between savanna fires, which burn primarily grass and leaf litter (Bond 1997; Scholes *et al*. 1996; van Wilgen and Scholes 1997; Williams *et al*. 2002), and forest and shrubland fires, which burn not only fine fuels but also larger woody plant materials. A consequence of savanna fires burning relatively small amounts of predominantly fine fuels is that combustion products are easily scattered by wind, and the diagnostic spectral signal caused by charcoal deposition fades out quickly. Scholes and Walker (1993) reported a recovery to pre-fire albedo values 6 weeks after a fire in a southern Africa savanna. Frederiksen *et al*. (1990) noticed a rapid increase in visible and NIR reflectance, and in values of the normalized difference vegetation index (NDVI) after a savanna fire in West Africa. Ash and charcoal residue were dispersed by wind and bare soil and dry leaves became the dominant spectral features. Eleven days after the fire, red reflectance, NIR reflectance, and NDVI had recovered to 75%, 55%, and to 45% of their pre-fire levels. Frederiksen *et al*. (1990) highlighted the need for frequent imaging of the savanna biome during the fire season, in order to retain a large spectral difference between burned and unburned areas.

Eva and Lambin (1998*b*) analysed the temporal evolution of the spectral contrast between burned areas and unburned woodland savanna in Central Africa, using the

Table 1. Biomass and combustion completeness in some tropical savanna fire experiments

Location/ecosystem	Pre-fire biomass ($t\,ha^{-1}$)	Combustion completeness	Biomass consumed ($t\,ha^{-1}$)	Reference
Savanna grasslands with scattered shrubs, Brazil	7.6	0.91	6.9	Miranda *et al*. (1996)
	9.9	0.93	9.2	
	6.7	0.81	5.4	
	8.9	0.94	8.4	
Savanna woodlands, Zambia	5.8	0.74	4.3	Shea *et al*. (1996)
	5.1	0.88	4.5	
Savanna woodlands, Zambia	9.0	0.01	0.1	Hoffa *et al.* (1999)
	11.4	0.22	2.5	
	9.2	0.17	1.6	
	9.0	0.28	2.5	
	13.2	0.21	2.8	
	11.2	0.47	5.3	
Hydromorphic grasslands, Zambia	3.3	0.52	1.7	Hoffa *et al.* (1999)
	3.2	0.44	1.4	
	2.4	0.78	1.9	
	3.0	0.88	2.6	
	2.7	0.87	2.4	
	1.9	0.73	1.4	
	3.2	0.98	3.1	
Hydromorphic grasslands, Zambia	4.5	0.85	3.8	Pereira *et al.* (unpublished)
	4.9	0.89	4.4	
	5.1	0.82	4.2	
Savanna woodland, Zambia	4.5	0.41	1.8	Pereira *et al*. (unpublished)
Eucalypt savanna woodlands, Australia	5.6	0.91	5.1	Hurst *et al*. (1994)
Eucalypt savanna woodlands, Australia	8.0	0.88	7.0	Beringer *et al*. (2002)

Jeffries-Matusita (J-M) distance (Jensen 1996) and data from various sensors. With all Along Track Scanning Radiometer (ATSR-1) channels (1.6 μm, 3.7 μm, 11 μm, and 12 μm), they found that J-M distance values distance dropped from 1.414 immediately after the fire to 1.25, 17 days after the fire, and ∼1.1, 5 weeks after the fire. The upper bounds of error probability in the discrimination between burned and unburned surface for these values of J-M distance are 0%, 11% and 20%, respectively, using the approach of Swain (1978) to convert J-M distance into classification error probability.

Trigg and Flasse (2000) characterised the spectral–temporal response of burned savanna in Namibia using field spectroradiometry. Pre-fire fuel loading at the site was $0.35\,t\,ha^{-1}$ of grass biomass. Thirteen days after the fire, the spectral signature of the burn was still significantly different from that of an unburnt control plot in the thermal infrared domain (6–14 μm), and in the reflective domain at 2.1 μm, 1.24 μm, and 0.86 μm. The spectral reflectance difference was not statistically significant at 0.65 μm, 1.64 μm, 0.55 μm, and 0.47 μm. These findings of the reduced usefulness of the visible spectral range, and to a lower extent of the 1.64 μm region to detect burns confirm the results described in Pereira *et al*. (1999*c*). Trigg and Flasse (2000) also observed that the reflectance of burned surfaces in their study area approaches that of bare soil about 1 month after the fire.

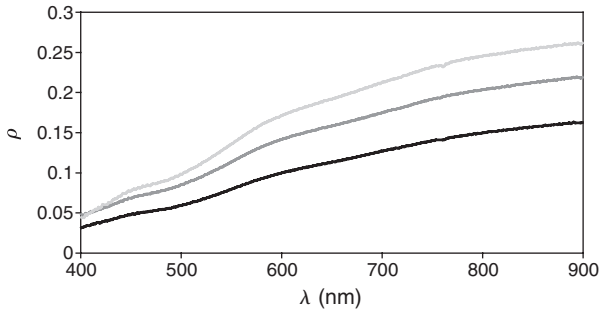

Fig. 4. Post-fire dynamics of the spectral reflectance (ρ) signature of a burned area in an hydromorphic grassland in the Western Province, Zambia (Sá *et al*. 2002*b*). Upper line, 1 September; centre line, 28 August; lower line, 25 August.

Figure 4 shows the rapid increase in reflectance after an experimental fire carried out 25 August 2000 in an hydromorphic grassland in western Zambia. Spectral reflectance of 16 circular quadrats (50 cm diameter) was measured using a FieldSpec VNIR spectroradiometer (Analytical Spectral Devices, Boulder, CO), over the range 0.350 m to 1.050 m, with a 1.4 nm sampling interval. At the beginning and at the end of each set of measurements, the reflectance of a white Spectralon reference plate was measured, to estimate solar irradiance at the surface and allow for the calculation of reflectance factors at each quadrat (Sá *et al*. 2003*b*). The spectral signature dated 25 August was measured ∼15 min after

the fire, and it is a mixture of the spectral signatures of charcoal and bare soil. The dominant *Loudetia simplex* grass tufts burned thoroughly and left a dark charcoal deposit but, in the spaces between tufts, bare soil was visible. In the subsequent measurements, the fraction of the surface covered by charcoal had decreased, and mean spectral reflectance over the 50 m transect used for the spectroradiometric measurements increased rapidly.

In temperate and boreal forests and shrublands the spectral signature of burned areas is more persistent than in tropical savannas because more biomass is burned and substantial amounts of large charred plant materials are left on the ground as combustion products. Lower net primary production delays the regrowth of vegetation, leaving a fire 'scar' which may be detectable for years to decades after the fire. Thus, it is feasible to wait for the end of the fire season to map the burns of the previous months. This option is not viable in tropical savannas, and burned area mapping methodologies need to rely on frequent imaging of the surface.

Cloud cover and multitemporal image compositing for burned area mapping

The probability of viewing clouds at any moment in time when observing the Earth from space is 0.62 for the northern hemisphere and 0.53 for the southern hemisphere, corresponding to a global mean probability of 0.575 (WMO 1994). Thus, cloud cover frequently prevents observation of the Earth surface from satellite. Vegetation fires generally occur during the local dry season, when cloud cover is relatively low, but in some areas it may still be problematic. In the tropics, cloud amount is high in the intertropical convergence zone and seasonal variations of tropical cloudiness track the shifting position of this zone. Data from the International Satellite Cloud Climatology Project (ISCCP) for the period 1993–1998 show that cloud cover is higher over the South American savannas than over southern African and Australian savannas during the months of June–November, which correspond to the drier part of the year in the southern hemisphere. In the northern hemisphere tropics, southern Asia is cloudier during the dry season than the savannas located between the Sahara desert and the equatorial rainforest of central Africa (http://isccp.giss.nasa.gov/climanal1.html).

Difficulties in obtaining cloud-free data with the required temporal resolution over very large areas, such as those affected by fire in tropical savannas, stimulated the development of multitemporal image compositing techniques. Image compositing is a procedure in which co-registered images acquired during a given period are combined in a way that the maximum or minimum of a chosen measurement (e.g. a vegetation index, reflectance of a single channel, or temperature) is selected as representative of the surface conditions during the period (Cracknell 1997). The most commonly used algorithm is maximum value compositing of the Normalized Difference Vegetation Index (MNDVI), a procedure developed by National Aeronautics and Space Administration Goddard Space Flight Center (NASA/GSFC) in the early 1980s (Tucker 1996), for which Holben (1986) established the scientific basis. In a multitemporal image mosaic constructed with the MNDVI, each pixel contains the maximum NDVI value observed at that pixel during the compositing period.

Cahoon *et al*. (1994), Martín (1998), Barbosa *et al*. (1998) and Sousa (1999) found that other compositing approaches are much better for burned area mapping than MNDVI, because recently burned surfaces have lower NDVI values than green vegetation, and will not appear in a composite image if a date with green vegetation is available during the compositing period. A worst case scenario happens when the first day of a compositing period is selected by the MNDVI because a fire occurred during the second day. When this happens the last day of the following compositing period gets selected, because the vegetation will have had more time to recover, increasing NDVI. This creates a gap of $2n - 1$ days (where n is the length of the compositing period, in days) between successive observations (Barbosa *et al*. 1998). Even with a relatively small n, the burn signal is strongly attenuated by the time it is picked up by the MNDVI, and detection of the burn is delayed by one compositing period. Barbosa *et al*. (1998) compared the performance of various compositing periods in terms of spectral detectability of the burn signal, and of viewing geometry of the composite images. They concluded that the MNDVI is not an appropriate compositing algorithm for mapping burns.

Sousa *et al*. (2003) confirmed previous findings about the unsuitability of the NDVI maximum value compositing algorithm for burned area mapping. They found that alternative algorithms, which increase the J-M distance between the spectral signatures of burned and unburned areas in composite images yielded better results. Sousa *et al*. (2003) demonstrated that the use of two-criteria compositing algorithms based on the sequential application of minimization of NIR reflectance, or of a combination of visible and NIR reflectance, followed by maximization of brightness temperature, solves the problem of cloud shadow retention which affects some of the simpler alternative algorithms.

These findings were derived from analysis of NOAA/AVHRR data, but ought to be applicable to imagery from other sensors with channels in the visible, NIR, and thermal domains, such as Moderate Resolution Imaging Spectrometer (MODIS) and the Advanced Along Track Scanning Radiometer (AATSR). The Vegetation (VGT) instrument, on-board the Système Probatoire d'Observation de la Terre (SPOT-4 and -5) satellites lacks a thermal sensor, which makes it harder to eliminate cloud shadows on composite images. Stroppiana *et al*. (2002) and Cabral *et al.* (2002) have developed techniques based on tracking the temporal persistence of very dark pixels. These are very effective at separating recent burns from cloud shadows, and produce composite images with very good observation geometry and almost free from

spatial heterogeneity artifacts. A remaining problem with these algorithms is their inability to eliminate persistent shadows cast by topographic features.

Image compositing strongly reduces the radiometric variability of a time-series of satellite data induced by changes in atmospheric conditions and viewing/illumination geometry. Therefore, it contributes to increase the accuracy of burned area mapping by supervised image classification approaches (Stroppiana *et al*. 2002). However, instead of attempting to suppress the variation in surface reflectance as a function of viewing/illumination geometry (i.e. the Bidirectional Reflectance Distribution Function, BRDF), this information may be used to derive adaptive approaches to burned area mapping (Roy *et al*. 2002).

The research by Barbosa *et al*. (1998), Sousa *et al*. (2003), Stroppiana *et al*. (2002), and Cabral *et al.* (2002) deals with regions containing extensive areas of savanna, and may contribute towards improved approaches for inter-tropical burned area mapping.

The effect of smoke on the detection of burned surfaces

The short duration of the burned area signal of tropical savanna fires imposes the need to monitor burning at a high frequency during the dry season. However, the large amounts of biomass burned in tropical savannas produce abundant emissions of smoke aerosols, which affect observation of the land surface from satellite. Lobert *et al.* (1999) estimated annual global emissions of C from biomass burning at 3716 TgC. Tropical biomass burning, including savanna fires, deforestation, and slash burning/shifting cultivation emits 2007 TgC yr^{-1}, or 53.9% of the total. According to Dickinson (1993), 3% of the C emitted goes into smoke, implying that tropical biomass burning produces 60.21 Tg of smoke aerosols per year.

Mie scattering is maximum when the particle radius corresponds to the wavelength of radiation. Smoke aerosol particles range in size from 0.01 to 1.0 μm, which makes them efficient scatterers of solar radiation (Jacob 1999). Biomass burning smoke is also an absorbing aerosol, because it contains high concentrations of black carbon (Dubovik *et al*. 2002; Kaufman *et al*. 2002). Aerosol optical thickness, $\kappa_{a\lambda}$, measures the attenuation of radiation propagating through the atmosphere. It depends on the aerosol optical characteristics and on total aerosol loading (Kaufman 1989). Since the attenuation effects of scattering and absorption are difficult to separate, $\kappa_{a\lambda}$ can be characterized with a single formula, known as Ångstrom's turbidity formula (Iqbal 1983):

$$\kappa_{a\lambda} = \beta\lambda^{-\alpha 125},$$

where β is known as Ångstrom's turbidity coefficient and represents the amount of aerosols present in the atmosphere in the vertical direction. The exponent α (or Ångstrom parameter) characterizes the size distribution of aerosol particles, and larger values of α indicate a relatively higher ratio of small particles to large particles. λ denotes the wavelength of radiation, in μm.

Dubovik *et al*. (2002) refer a range of $\kappa_{a0.44}$ values from 0.1 to 3 for the Amazon forest, and of 0.1 to 2.1 for woody savanna (*cerrado*) in Brazil, during the period August–October, i.e. the peak of the fire season. Typical α values are in the range 1.2–2.1. During the late dry season (August–November) in the savannas of Zambia, $\kappa_{a0.44}$ varied from 0.1 to 1.5, and α varied between 1.4 and 2.2. The smoke aerosol data of Holben *et al*. (2001) show that at Cuiabá, Brazil, $\kappa_{a0.5}$ peaks in September with a mean monthly value of ∼1.2, and the highest α mean monthly values are of ∼1.7 in August and September. In Mongu, Zambia, September is also the month with the highest mean $\kappa_{a0.5}$, but the value is 0.6, much lower than in Brazil. The Ångstrom parameter, α, in Mongu stays between 1.7 and 1.9 from June through October. Higher smoke aerosol loadings in Brazil than in Zambia may be due to the burning of larger amounts of biomass and/or to differences in atmospheric circulation patterns. The higher values of α observed in Zambia indicate that the median radius of particles is smaller for African smoke than from smoke in the Amazon. Dubovik *et al*. (2002) consider that larger-sized smoke particles in forested regions may result from a greater proportion of biomass being consumed in smoldering combustion. It has been estimated that, in savanna ecosystems, ∼85% of the biomass is consumed by flaming combustion, while for deforestation fires the percentage may be 50% or less (Ward *et al*. 1996).

The perturbation caused by smoke aerosol to observation of the land surface from satellite can be quantified calculating the aerosol transmittance, $\tau_{a\lambda}$ (Iqbal 1983):

$$\tau_{a\lambda} = \exp(-\beta\lambda^{-\alpha} m_a),$$

where m_a is the optical mass of air. Values of $\kappa_{a\lambda}$ and corresponding α values are given by Eck *et al*. (1998) for the Brazilian Amazon, and by Eck *et al*. (2001) for Zambia. Figure 5 illustrates the strong dependence of aerosol transmittance on wavelength, using as an example measurements taken on 4 September 1995, a day of extremely high $\kappa_{a0.44}$ in the Brazilian Amazon (table 9*b* in Eck *et al*. 1998) and on 10 September 1997 in Mongu, Zambia, under less extreme conditions and with κ_a measured at 0.5 μm. A solar zenith angle of 30° was assumed in both cases, corresponding to an m_a value of 1.15.

Figure 5 shows how τ_a increases non-linearly with λ, in both the Brazil (dashed line), and Zambia (solid line) cases. The vertical bars represent the approximate spectral location of the Landsat ETM+ reflective channels. Aerosol transmittance in the visible spectral domain, represented by channels 1–3, does not exceed 0.1 for the Brazil example, meaning that the smoke aerosol almost completely obstructs observation of the land surface. Transmittance in the visible does not exceed 0.5 in the Zambia example. In the mid-infrared

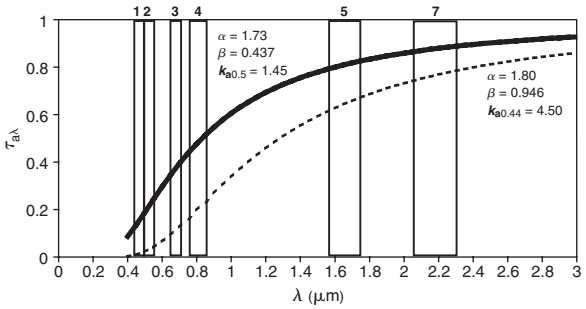

Fig. 5. Atmospheric transmittance as a function of wavelength, for smoke aerosol layers observed in Brazil and in southern Africa. The vertical bars represent the approximate spectral position of the Landsat 7 Enhanced Thematic Mapper (ETM+) sensor.

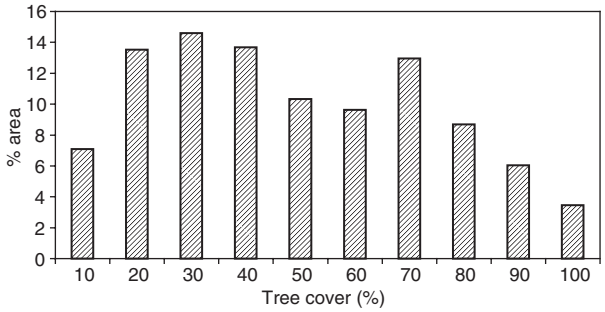

Fig. 6. Percentage of the area of tropical savannas by tree canopy cover class. Values in the abcissa represent the upper limit of the class.

domain (channels 5 and 7), transmittance is much higher, reaching almost 90% for the African smoke aerosol in ETM+ channel 7. A clear implication of these results is that the visible spectral domain is inadequate to monitor the land surface in tropical environments, when smoke aerosol from biomass burning is present in the atmosphere in significant amounts, and ought to be replaced with mid-infrared data, namely for the detection and mapping of burned surfaces (Pereira 1999). Kaufman *et al*. (1997) showed that there is a good correlation between surface reflectance in the red or blue spectral regions, and reflectance in the mid-infrared at 2.2 μm, and that detection of dark surface pixels can be effectively accomplished with mid-infrared data. The physical basis of the correlation between the visible and mid-infrared spectral domains is also discussed by Kaufman *et al*. (1997). Development of the GEMI3 index by Pereira (1999), as a modification of the Global Environment Monitoring Index (GEMI) of Pinty and Verstraete (1992) represents an implementation of this concept for burned area mapping, which was also successfully implemented in a tropical savanna region (Pereira *et al*. 1999*a*).

Detectability of understory burns

Surface fires predominate in savanna ecosystems, where trees are normally not part of the fuel complex (Bond 1997), although understory fires may scorch tree canopies (Bond and van Wilgen 1996; Williams *et al*. 2002). Understory burns may be difficult to detect from space due to the interception of radiation and casting of shadows by the overstory layer. Detection of understory burns is expected to be more problematic in areas of dense tree cover and high leaf area index (LAI), unless fire causes trees to shed foliage.

Leaf area index of tropical savannas and woody savannas displays strong seasonal variability. Fires in general, and especially late dry season fires, occur during the period when LAI is lower, which ought to facilitate detection of understory burning. The mean annual LAI map for the period 1981–1991 derived by Buermann *et al.* (2002) shows that the highest LAI values in tropical savannas are found in the woody savannas of southern Africa, namely in the southern Democratic Republic of Congo, northern Zambia, and north-eastern Angola. LAI of savanna ecosystems is constrained by tree percentage cover, if considered at the landscape level observed from coarse spatial resolution satellite sensors. Tree percentage cover does not vary seasonally and is easier to use to identify areas where detection of understory burns may be problematic. Figure 6 shows the distribution of tree cover in the area defined as savanna for the purposes of this study. The tree cover data are from the 1 km spatial resolution Global Forest Canopy Density (GFCD) map produced by the United Nations Food and Agriculture Organization (FAO) under the Global Forest Resources Assessment (FRA2000) initiative (http://edcdaac.usgs.gov/glcc/fao/index.html).

According to the definition of the IGBP-DIS Land Cover Classification, the tree cover of woody savannas varies from 30% to 60% (Scepan 1999), but the GFCD map shows that ~30% of the area of savannas and woody savannas has tree cover higher than 60%. Those are the conditions under which detection of understory burning may be problematic. Below that threshold, Fuller *et al*. (1997), analysed the influence of canopy strata on the remotely sensed signal of savanna woodlands from eastern Zambia. They found that the understory layer dominated the remotely sensed signal throughout most of the seasonal cycle, because of high tree canopy transmittance, heterogeneous tree cover, and lower reflectance of the tree layer relative to the grassy understory. Their simulations performed with the SAIL model (Verhoef 1984) suggest that the tree canopy layer makes a relatively small contribution to landscape-scale normalized difference vegetation index (NDVI), for tree cover values of up to 60%. The radiometric contribution from the tree layer tends to be relatively more important during the dry season, when at least part of the understory vegetation is senescent.

Pereira *et al*. (unpublished data) assessed the detectability of understory burns in wetter Zambezian miombo woodlands (White 1983), considering the spectral and structural properties of tree stands and of the surface vegetation layer before and after the fire. The problem was analysed with

a simulation approach, using an analytical hybrid geometric optical (GO) and radiative transfer (RT) model (Ni *et al*. 1999) and a combination of satellite data, field spectroradiometric and biometric data. Pereira *et al*. (unpublished data) found that recently burned sites are easily separated from unburned sites using spectral data in the green, red, and near-infrared (NIR) domains. Discrimination of older burns is also possible, but with lower accuracy. Simulation results were highly insensitive to variation in stand structure parameters, and responded almost exclusively to differences in the spectral characteristics of the simulated scene background. The effect of viewing geometry was not analysed, since all model runs were performed assuming nadir viewing. The simulations were performed with data representative of the wetter Zambezian miombo woodlands, and a maximum tree cover of 60%. Since spectral detectability of understory burns was found to be very high even at 60% canopy cover, it may remain feasible even at higher canopy densities. However, it is important to acquire field and satellite data representative of dense woody savannas in order to test that hypothesis. Further research on this topic would benefit from using more sophisticated radiative transfer models such as the discrete anisotropic radiative transfer (DART) model of Gastellu-Etchegorry *et al*. (1996), which has already been used to analyse the dependence of canopy reflectance of tropical forests on the structure and optical properties of understory vegetation (Gastellu-Etchegorry *et al*. 1999). Analysis of the detectability of burned areas in the understory of woody savannas can contribute towards the development of better algorithms and more accurate estimates of error for burned area mapping studies in tropical regions.

Capabilities and limitations of major sensors

Currently available coarse spatial resolution sensors are considered adequate to monitor tropical savanna fires with the frequency and accuracy required, not only for estimation of atmospheric emissions and impacts on terrestrial ecosystems, but also for various operational applications in fire management (Pereira *et al.* 2001). Table 2 shows the main instrument specifications relevant for burned area mapping.

The on-going Global Burned Areas 2000 initiative of the Institute for the Environment and Sustainability/Joint Research Centre (IES/JRC) (http://www.gvm.sai.jrc.it/fire/gba2000_website/index.htm) is mapping the areas burned globally during the year 2000. Burned area maps are produced on a monthly basis and at 1 km spatial resolution, using data from the VGT instrument (Grégoire *et al.* 2003). A significant strength of VGT is the reduced pixel distortion towards edge of swath and the excellent coregistration between dates (Vegetation User Guide, http://vegetation.cnes.fr/userguide/userguide.htm). However, VGT lacks a channel in the thermal domain, which is useful to discriminate between recent burns and other dark surfaces, such as cloud shadows and water bodies. This limitation, as already mentioned, requires somewhat more complex multitemporal compositing approaches for burned area analyses.

MODIS has good spectral resolution, with seven channels, including a 1.24 μm channel not available in any other sensor and useful for the detection and mapping of burned areas (Sá *et al*. 2003*a*). Spatial resolution of the 0.65 μm and 0.86 μm channels is 250 m, while that of the other five channels listed in Table 2 is 500 m. The 2.13 μm channel of MODIS is excellent for observing the surface through smoke-filled atmospheres, although the channels located at ∼1.6 μm available in all other sensors, are also very appropriate as shown in Fig. 5. A second MODIS instrument was successfully launched 4 May 2002 on board the Aqua spacecraft, thus doubling the temporal resolution of MODIS Earth observation.

A limitation of the AATSR is its lower temporal resolution. It takes the AATSR about 2 months to acquire the same number of observations of a tropical area that the other sensors acquire in 10–15 days. Therefore, it is probably unfeasible to produce pan-tropical burned area maps with the AATSR at a temporal resolution better than 2 months.

The spatial resolution listed in Table 2 refers to the ideal situation of a nadir view, but pixel size increases towards the edge of the sensor swath. This loss of spatial resolution is more severe in the wide-swath scanning mirror sensors, namely the AVHRR and MODIS. At a 55° scan angle, corresponding to the edge of swath for both instruments, the AVHRR pixel size increases to 6.5 km × 2.3 km (Goodrum *et al*. 2000) and the MODIS 500 m pixel size increases to 4.8 km × 2 km (Nishihama *et al*. 1997). The AATSR is less affected by this problem, because it has a much narrower swath, of ∼500 km. VGT uses push-broom scanning, rather than a scanning mirror, and maintains excellent spatial resolution up to the edge of swath, where pixel size is ∼1.4 km × 1.4 km (Vegetation User Guide). Thus, the AATSR and VGT sensors are capable of consistently detecting smaller burns than the AVHRR. Close to nadir, MODIS has better spatial resolution than the AATSR and VGT, but for off-nadir viewing angles these instruments outperform MODIS.

The Medium Resolution Imaging Spectrometer (MERIS) is a push-broom imaging spectrometer that was recently launched (March 1 2002) aboard the ENVIronment SATellite (ENVISAT). MERIS has a spatial resolution of 300 m at nadir in full resolution mode. Pixel size is reduced to 1200 m by the on-board combination of four adjacent samples across track over four successive lines. The instrument's 1150 km swath width allows for global coverage in 3 days. MERIS has 15 spectral channels positioned between 0.4 μm and 15 μm, programmable in width and position (Rast and Bézy 1999; Bézy *et al*. 2000). The lack of spectral channels over the mid-infrared and thermal domains is a disadvantage for mapping burned areas (Pereira 1999; Pereira *et al*. 1999*c*).

Table 2. Specifications of the main sensors available for broad area mapping of burns in tropical savannas

	Resolution				
Sensor	Spatial (km, at nadir)	Temporal[A]	Spectral channels (μm)	Radiometric[B]	Angular
AVHRR/3	1	1	0.63, 0.86, 1.62[C], 10.8, 12	1024	Single
VGT	1	1–2[D]	0.45, 0.65, 0.83, 1.65	4096	Single
MODIS	0.25[E]–0.5	1–2[D]	[F]0.65, 0.86, 0.47, 0.56, 1.24, 1.64, 2.13	4096	Single
AATSR	1	4–5[D]	0.55, 0.66, 0.87, 1.6[C], 11, 12	4096	Dual
MERIS	0.3[G]	3	0.39–1.04[H]	4096	Single
MISR	0.275[I]	9	0.446, 0.558, 0.672, and 0.867	4096	0°, 26.1°[J], 45.6°, 60°, 70.5°

[A] Number of days required for global coverage.
[B] Refers to the maximum number of grey levels in an image.
[C] Channel available during daytime only. At night it is replaced by a 3.7 μm channel.
[D] The lower frequency of observation (2 or 5 days) occurs in the intertropical belt.
[E] For 0.65 μm and 0.86 μm channels only.
[F] Land surface observation channels. MODIS has a total of 36 channels.
[G] This resolution is reduced to 1200 m by the on board combination of four adjacent samples across track over four successive lines.
[H] 15 channels within the range, programmable in width and position.
[I] Data averaged in 4 × 4, 1 × 4, or 2 × 2 pixels, individually selected for each camera and spectral band.
[J] The non-nadir angles are available in fore and aft cameras, for a total of nine views.

The Multi-angle Imaging SpectroRadiometer (MISR, Diner *et al*. 1998, 1999), aboard the Terra spacecraft, is a push-broom instrument with nine cameras pointed at fixed view angles, ranging from 0° to 70.5°. Each camera obtains imagery in four spectral bands—blue, green, red and NIR. The MISR cross-track swath width of 360 km allows viewing the entire Earth's surface every 9 days. In local mode, selected targets 300 km long will be imaged at the maximum spatial resolution of 275 m. Away from these targets (only about six per day), MISR operates in global mode, which averages data in 4 × 4, 1 × 4, or 2 × 2 pixels, individually selected for each camera and spectral band. The nine different look angles allow for good characterization of the BRDF, leading to very powerful methods for detecting land-cover changes, namely those induced by vegetation burning. The cameras at 45.6° angles (fore and aft) are included for sensitivity to aerosol properties, while the cameras at 60° are particularly important for the estimation of hemispherical albedo. MISR lacks spectral channels over the mid-infrared and thermal domains. Acquisition of cloud-free data over many tropical regions may be problematic, due to the instrument's nine day repeat cycle.

Geostationary instruments have not been extensively used for burned area mapping, although the Geostationary Operational Environmental Satellite (GOES) has been used for active fire and smoke detection and mapping (Menzel and Prins 1996). The studies of fire-induced albedo changes in Africa (Govaerts *et al.* 2002), which used METEOrological SATellite (METEOSAT) data, and Boschetti *et al*. (2001), based on METEOSAT and Geostationary Meteorological Satellite (GMS) are exceptions to this trend. The potential of METEOSAT Second Generation (MSG-1), launched in August 2002, for fire applications in Africa and southern Europe is very good due to improved spatial, spectral, and temporal resolutions (Pereira and Govaerts 2001). Development of a relatively long-term (20 years) dataset of areas burned in tropical savannas is important because it is required to quantify fire return intervals and interannual variability of fire incidence. It can only be accomplished with Global Area Coverage (GAC) data from the AVHRR, at 4 km resolution (Gutman *et al*. 2000), or using the Pathfinder dataset (Agbu and James 1994). Barbosa *et al*. (1999*b*) demonstrated the feasibility of this task, with an 8-year analysis of burned areas, burned biomass, and atmospheric emissions over Africa, based on the previous development of algorithms for multitemporal image compositing (Barbosa *et al*. 1998), and for classification of time-series data (Barbosa *et al*. 1999*a*). Development of a 20-year global burned areas dataset based on AVHRR-GAC data is a challenge which ought to be undertaken soon by the research community involved in remote sensing of fire.

Conclusions

Tropical savannas are the most fire-prone biome on Earth, and the largest source of atmospheric emissions from biomass burning. The magnitude and importance of the atmospheric, climatic and ecological impacts of tropical savanna fires justifies the need for timely and accurate monitoring of the spatio-temporal patterns of fire occurrence. Given the extent of the areas affected, satellite remote sensing is the only viable option for pan-tropical mapping of areas burned by savanna fires. Attributes of fires in tropical savannas which are relevant to detecting and mapping burned areas from space include:

- Heterogeneity of fire-induced spectral changes;
- Ephemeral nature of the charcoal deposition signal;

- Importance of multitemporal image compositing;
- Difficulties introduced by the presence of clouds and smoke; and
- Detectability of understory burns.

Recent research dealing with these topics was reviewed and recommendations were provided for the development of algorithms adequate to handle the specific situations of burned area mapping from satellite under the conditions commonly found in tropical savannas. The main coarse spatial resolution sensors adequate for pan-tropical coverage, although not ideally suited for fire monitoring and mapping, provide data which can be used to map burned areas at spatial and temporal resolutions appropriate for monitoring the major environmental impacts of tropical savanna fires, and for supporting operational fire management activities.

Acknowledgements

This research is part of Project POCTI/CTA/33582/99 (*Reduction of uncertainties in estimates of atmospheric emissions from fires in southern Africa*), Foundation for Science and Technology, Ministry for Science and Technology, Portugal. I am grateful to Bernardo Mota and Ana Sá (Department of Forestry, Instituto Superior de Agronomia) for preparing the figures.

References

Agbu PA, James ME (1994) 'The NOAA/NASA Pathfinder AVHRR Land Data Set User's Manual.' Goddard Distributed Active Archive Center, NASA. (Goddard Space Flight Center: Greenbelt, MD)

Andreae MO (1997) Emissions of trace gases and aerosols from southern African savanna fires. In 'Fire in southern African savannas: Ecological and atmospheric perspectives'. (Eds BW van Wilgen, MO Andreae, JG Goldammer and JA Lindesay) pp. 161–184. (Witwatersrand University Press: Johannesburg)

Barbosa PM, Pereira JMC, Grégoire J-M (1998) Compositing criteria for burned area assessment using multitemporal low resolution satellite data. *Remote Sensing of Environment* **65**, 38–49.

Barbosa PM, Grégoire J-M, Pereira JMC (1999*a*) An algorithm for extracting burned areas from time series of AVHRR GAC data applied at a continental scale. *Remote Sensing of Environment* **69**, 253–263.

Barbosa PM, Grégoire J-M, Stroppiana D, Pereira JMC (1999*b*) An assessment of fire in Africa (1981–1991): burnt areas, burnt biomass and atmospheric emissions. *Global Biogeochemical Cycles* **13**, 933–950.

Beringer J, Hutley LB, Tapper NJ, Coutts A, Kerley A, O'Grady AP (2003) Fire impacts on surface heat, moisture and carbon fluxes from a tropical savanna in northern Australia. *International Journal of Wildland Fire* **12**, 333–340.

Bézy J-L, Delwart S, Rast M (2000) MERIS—A new generation of ocean-colour sensor onboard Envisat. *ESA Bulletin* **103**, 48–56.

Bond WJ (1997) Fire. In 'Vegetation of southern Africa'. (Eds RM Cowling, DM Richardson and SM Pierce) pp. 421–446. (Cambridge University Press: Cambridge, UK)

Bond W, van Wilgen BW (1996) 'Fire and plants.' (Chapman and Hall: London).

Boschetti L, Brivio PA, Grégoire J-M (2001) Detection of burned areas using geostationary satellite data in tropical environments. In 'Proceedings of the Symposium Remote Sensing for Agriculture, Ecosystems, and Hydrology'. 25–29 September 2000, Barcelona, Spain. (Eds M Owe, G D'Urso and E Zilioli) pp. 156–165. (International Society for Optical Engineering: Washington, D.C.)

Breiman L, Friedman JH, Olshen RA, Stone PJ (1984) 'Classification and regression trees.' (Wadsworth International Group: Belmont, CA)

Buermann W, Wang Y, Dong J, Zhou L, Zeng X, Dickinson RE, Potter CS, Myneni RB (2002) Analysis of a multi-year global vegetation leaf area index data set. *Journal of Geophysical Research–Atmospheres* (In press)

Cabral A, Vasconcelos MJP, Pereira JMC, Bartholomé E, Mayaux P (2002) Multitemporal compositing approaches for SPOT-4 VEGETATION data. *International Journal of Remote Sensing* (In press)

Cahoon DR, Stocks BJ, Levine JS, Cofer WR III, Pierson JM (1994) Satellite analysis of the severe 1987 forest fires in northern China and southeastern Siberia. *Journal of Geophysical Research* **99**, 18 627–18 638.

Cracknell AP (1997) 'The Advanced Very High Resolution Radiometer.' (Taylor and Francis: London)

Dickinson RE (1993) Effect of fires on global radiation budget through aerosol and cloud properties. In 'Fire in the environment'. (Eds PJ Crutzen and JG Goldammer) pp. 107–122. (John Wiley & Sons: Chichester)

Diner DJ, Beckert JC, Reilly TH, Bruegge CJ, Conel JE, *et al.* (1998) Multi-angle Imaging SpectroRadiometer (MISR) instrument description and experiment overview. *IEEE Transactions on Geoscience and Remote Sensing* **36**, 1072–1087.

Diner DJ, Asner GP, Davies R, Knyazikhin Y, Muller J-P, Nolin AW, Pinty B, Schaaf CB, Stroeve J (1999) New directions in Earth observing: Scientific applications of Multiangle Remote Sensing. *Bulletin of the American Meteorological Society* **80**, 2209–2228.

Dubovik O, Holben B, Eck TF, Smirnov A, Kaufman YJ, King MD, Tanré D, Slutsker Y (2002) Variability of absorption and optical properties of key aerosol types observed in worldwide locations. *Journal of the Atmospheric Sciences* **59**, 590–608.

Dwyer E, Pinnock S, Grégoire J-M, Pereira JMC (2000) Global spatial and temporal distribution of vegetation fire as determined from satellite observations. *International Journal of Remote Sensing* **21**, 1289–1302.

Eck TF, Holben BN, Slutsker I, Setzer A (1998) Measurements of irradiance attenuation and estimation of aerosol single scattering albedo for biomass burning aerosols in Amazonia. *Journal of Geophysical Research* **103**, 31 865–31 878.

Eck TF, Holben BN, Ward DE, Dubovik O, Reid JS, Smirnov A, Mukelabai MM, Hsu NC, O'Neill NT, Slutsker I (2001) Characterization of the optical properties of biomass burning aerosols in Zambia during the 1997 ZIBBEE field campaign. *Journal of Geophysical Research* **106**, 3425–3448.

Eva H, Lambin EF (1998*a*) Burnt area mapping in Central Africa using ATSR data. *International Journal of Remote Sensing* **19**, 3473–3497.

Eva H, Lambin EF (1998*b*) Remote sensing of biomass burning in tropical regions: sampling issues and multisensor approach. *Remote Sensing of Environment* **64**, 292–315.

Fernandes PM, Catchpole WR, Rego FC (2000) Shrubland fire behaviour modelling with microplot data. *Canadian Journal of Forest Research* **30**, 889–899.

FIRESCAN Science Team (1996) Fire in ecosystems of boreal Eurasia: The Bor Forest Island Fire Experiment, Fire Research Campaign Asia-North (FIRESCAN). In 'Biomass burning and global change, Vol. II'. (Ed. JS Levine) pp. 848–873. (MIT Press: Cambridge, MA)

Flasse SP, Ceccato P (1996) A contextual algorithm for AVHRR fire detection. *International Journal of Remote Sensing* **17**, 419–424.

Frederiksen P, Langaas S, Mbaye M (1990) NOAA-AVHRR and GIS-based monitoring of fire activity in Senegal—a provisional methodology and potential applications. In 'Fire in tropical biota'. (Ed. JG Goldammer) pp. 400–417. (Springer-Verlag: Berlin)

French NHF, Kasischke ES, Stocks BJ, Mudd JP, Martell DL, Lee BS (2000) Carbon release from fires in the North American boreal forest. In 'Fire, climate change, and carbon cycling in the boreal forest'. (Eds ES Kasischke and BJ Stocks) pp. 377–388. (Springer-Verlag: New York)

Fuller DO, Prince SD, Astle WL (1997) The influence of canopy strata on remotely sensed observations of savanna-woodlands. *International Journal of Remote Sensing* **18**, 2985–3009.

Gastellu-Etchegorry J, Demarez V, Pinel V, Zagolski F (1996) Modeling radiative transfer in heterogeneous 3-D vegetation canopies. *Remote Sensing of Environment* **58**, 131–156.

Gastellu-Etchegorry JP, Guillevic P, Zagolski F, Demarez V, Trichon V, Deering D, Leroy M (1999) Modeling BRF and radiation regime of boreal and tropical forests: I. BRF. *Remote Sensing of Environment* **68**, 281–316.

Goodrum G, Kidwell KB, Winston W (Eds) (2000) 'NOAA KLM User's Guide, September 2000 Revision.' (NOAA/NESDIS: Suitland, MA)

Govaerts YM, Pereira JMC, Pinty B, Mota B (2002) Impact of fires on surface albedo dynamics over the African continent. *Journal of Geophysical Research–Atmospheres* **107**(D22), 4629.

Grégoire J-M, Tansey K, Silva JMN (2003) The GBA2000 initiative: Developing a global burnt area database from SPOT-VEGETATION imagery. *International Journal of Remote Sensing* **24**(6), 1369–1376.

Gutman G, Elvidge C, Csiszar I, Romanov P (2000) NOAA archives of data from meteorological satellites useful for fire products. In 'Global and regional wildfire monitoring from space: Planning a coordinated international effort'. (Eds FJ Ahern, J Goldammer and C Justice) pp. 257–265. (SPB Academic Publishing: The Hague)

Hlavka CA, Ambrosia VG, Brass JA, Rezendez AR, Guild LS (1995) Mapping fire scars in the Brazilian cerrado using AVHRR imagery. In 'Biomass burning and global change, Vol. II'. (Ed. JS Levine) pp. 555–560. (MIT Press: Cambridge, MA)

Hoffa EA, Ward DE, Hao W-M, Susott RA, Wakimoto RH (1999) Seasonality of carbon emissions from biomass burning in a Zambian savanna. *Journal of Geophysical Research* **104**, 13 841–13 853.

Holben BN (1986) Characteristics of maximum-value composite images from temporal AVHRR data. *International Journal of Remote Sensing* **7**, 1417–1434.

Holben BN, Tanré D, Smirnov A, Eck TF, Slutsker I, *et al*. (2001) An emerging ground-based aerosol climatology: Aerosol optical depth from AERONET. *Journal of Geophysical Research* **106**, 12 067–12 098.

House JI, Hall DO (2001) Productivity of tropical savannas and grasslands. In 'Terrestrial global productivity'. (Eds J Roy, B Saugier and HA Mooney) pp. 363–400. (Academic Press: San Diego)

Hurst DF, Griffith DWT, Cook GD (1994) Trace gas emissions from biomass burning in tropical Australian savannas. *Journal of Geophysical Research* **99**, 16 441–16 456.

Iqbal M (1983) 'An introduction to solar radiation.' (Academic Press: Toronto)

Jacob DJ (1999) 'Introduction to atmospheric chemistry.' (Princeton University Press: Princeton)

Jensen JR (1996) 'Introductory digital image processing: A remote sensing perspective (2nd edn).' (Prentice-Hall: New York)

Kaufman Y (1989) The atmospheric effect on remote sensing and its corrections. In 'Theory and applications of optical remote sensing'. (Ed. G Asrar) pp. 336–428. (John Wiley & Sons: New York)

Kaufman YJ, Tanré D, Boucher O (2002) A satellite view of aerosols in the climate system. *Nature* **419**, 215–223.

Kaufman YJ, Wald AE, Remer LA, Gao B-C, Li R-R, Flynn L (1997) The MODIS 2.1-μm channel—Correlation with visible reflectance for use in remote sensing of aerosol. *IEEE Transactions on Geoscience and Remote Sensing* **35**, 1286–1298.

Keith DA, McCaw WL, Whelan RJ (2002) Fire regimes in Australian heathlands and their effects on plants and animals. In 'Flammable Australia: the fire regimes and biodiversity of a continent'. (Eds RA Bradstock, JE Williams and AM Gill) pp. 199–237. (Cambridge University Press: Cambridge, UK)

Lobert JM, Keene WC, Logan JA, Yevich R (1999) Global chlorine emissions from biomass burning: reactive chlorine emissions inventory. *Journal of Geophysical Research* **104**(D7), 8373–8389.

Martín MP (1998) Cartografía e inventario de incendios forestales en la Península Ibérica a partir de imágenes NOAA-AVHRR. Doctoral Thesis, Universidad de Alcalá, Departamento de Geografía: Alcalá de Henares, Spain.

Menzel WP, Prins EM (1996) Monitoring biomass burning with the new generation of geostationary satellites. In 'Biomass burning and global change, Vol 1'. (Ed. JS Levine) pp. 56–64. (MIT Press: Cambridge, MA)

Miller JD, Yool SR (2002) Mapping forest post-fire canopy consumption in several overstory types using multi-temporal Landsat TM and ETM data. *Remote Sensing of Environment* **82**, 481–496.

Miranda HS, Silva EPR, Miranda AC (1996) Comportamento do fogo em queimadas de campo sujo. In 'Impactos de Queimadas em Áreas de Cerrado e Restinga'. (Eds HS Miranda, CM Saito and BFS Dias) pp. 1–10. (University of Brasília: Brasília, Brazil)

Mitchell TM (1997) 'Machine learning.' (McGraw-Hill: New York)

Ni W, Li X, Woodcock CE, Caetano MR, Strahler AH (1999) An analytical hybrid GORT model for bidirectional reflectance over discontinuous plant canopies. *IEEE Transactions on Geoscience and Remote Sensing* **37**, 987–999.

Nishihama M, Wolfe R, Solomon D, Patt F, Blanchette J, Fleig A, Masuoka E (1997) MODIS Level 1A Earth Location: Algorithm Theoretical Basis Document Version 3.0. MODIS Science Data Support Team, SDST-092. (NASA Goddard Space Flight Center: Greenbelt, MD)

Pereira JMC (1999) A comparative evaluation of NOAA/AVHRR vegetation indexes for burned surface detection and mapping. *IEEE Transactions on Geoscience and Remote Sensing* **37**, 217–226.

Pereira JMC, Flasse S, Hoffman A, Pereira JAR, González-Alonso F, Trigg S, Vasconcelos MJP, Bartalev S, Lynham TJ, Korovin G, Lee BS (2001) Operational use of remote sensing for fire management: regional case studies. In 'Global and regional wildfire monitoring from space: Planning a coordinated international effort'. (Eds FJ Ahern, J Goldammer and C Justice) pp. 47–70. (SPB Academic Publishing: The Hague)

Pereira JMC, Govaerts Y (2001) Potential fire applications from MSG/SEVIRI observations. EUMETSAT Program Development Department Technical Memorandum No. 07. (EUMETSAT: Darmstadt)

Pereira JMC, Pereira BS, Barbosa PM, Stroppiana D, Vasconcelos MJP, Grégoire J-M (1999*a*) Satellite monitoring of the overall fire activity in the EXPRESSO study area during the dry season experiment: active fires, burnt areas, and atmospheric emissions. *Journal of Geophysical Research* **104**, 30 701–30 712.

Pereira JMC, Sá ACL, Sousa AMO, Silva JMN, Santos TN, Carreiras JMB (1999c) Spectral characterisation and discrimination of burnt

areas. In 'Remote sensing of large wildfires in the European Mediterranean Basin'. (Ed. E Chuvieco) pp. 123–138. (Springer-Verlag: Berlin)

Pereira JMC, Sousa AMO, Sá ACL (1999*b*) Regional scale burnt area mapping in Southern Europe using NOAA-AVHRR 1 km data. In 'Remote sensing of large wildfires in the European Mediterranean Basin'. (Ed. E Chuvieco) pp. 139–155. (Springer-Verlag: Berlin)

Pereira JMC, Vasconcelos MJP, Sousa AMO (2000) A rule-based system for burnt area mapping in temperate and tropical regions using NOAA/AVHRR imagery. In 'Biomass burning and its interrelationships with the climate system'. (Eds JL Innes, MM Verstraete and M Beniston) pp. 215–232. (Kluwer Academic Publishers: Dordrecht)

Pinty B, Verstraete MM (1992) GEMI: a non-linear index to monitor global vegetation from satellites. *Vegetatio* **101**, 15–20.

Rast M, Bézy J-L (1999) The ESA Medium Resolution Imaging Spectrometer MERIS: a review of the instrument and its mission. *International Journal of Remote Sensing* **20**, 1681–1702.

Robinson JM (1991) Problems in global fire evaluation: is remote sensing the solution? In 'Global biomass burning: Atmospheric, climatic, and biospheric implications'. (Ed. JS Levine) pp. 67–73. (MIT Press: Cambridge, MA)

Rogan J, Yool SR (2001) Mapping fire-induced vegetation depletion in the Peloncillo Mountains, Arizona and New Mexico. *International Journal of Remote Sensing* **22**, 3101–3121.

Roy DP, Giglio L, Kendall J, Justice CO (1999) Multitemporal active-fire based burn scar detection algorithm. *International Journal of Remote Sensing* **20**, 1031–1038.

Roy DP, Lewis PE, Justice CO (2002) Burned area mapping using multi-temporal moderate spatial resolution data—a bi-directional reflectance model-based expectation approach. *Remote Sensing of Environment* **83**, 263–286.

Sá ACL, Pereira JMC, Vasconcelos MJP, Silva JMN, Ribeiro N, Awasse A (2003*a*) Burned area mapping in the miombo woodland of northern Mozambique using MODIS and Lansat data. *International Journal of Remote Sensing* **24**(8), 1783–1796.

Sá ACL, Pereira JMC, Silva JMN (2003*b*) Estimation of combustion completeness based on fire-induced spectral reflectance changes in a *dambo* grassland in the Western Province, Zambia. *International Journal of Remote Sensing* (In press)

Scepan J (1999) Thematic validation of high-resolution global land-cover data sets. *Photogrammetric Engineering and Remote Sensing* **65**, 1051–1060.

Scholes RJ (1997) Savanna. In 'Vegetation of southern Africa'. (Eds RM Cowling, DM Richardson and SM Pierce) pp. 258–277. (Cambridge University Press: Cambridge, UK)

Scholes RJ, Kendall J, Justice CO (1996) The quantity of biomass burned in southern Africa. *Journal of Geophysical Research* **101**(23), 667–676.

Scholes RJ, Pickett G, Ellery WN, Blackmore AC (1997) Plant functional types in African savannas and grasslands. In 'Plant functional types'. (Eds TM Smith, HH Shugart and FI Woodward) pp. 255–268. IGBP Book Series No. 1. (Cambridge University Press: Cambridge, UK).

Scholes RJ, Walker BH (1993) 'An African savanna: Synthesis of the Nylsvley Study.' (Cambridge University Press: Cambridge, UK)

Shea RW, Shea BW, Kauffman JB, Ward DE, Haskins CI, Scholes MC (1996) Fuel biomass and combustion factors associated with fires in savanna ecosystems of South Africa and Zambia. *Journal of Geophysical Research* **101**, 23 551–23 568.

Siegert F, Hoffmann AA (2000) The 1998 Forest Fires in East Kalimantan (Indonesia). *Remote Sensing of Environment* **72**, 64–77.

Sousa AMO (1999) Desenvolvimento de uma metodologia para a cartografia de áreas ardidas superiores a 500 ha para a Península Ibérica com dados AVHRR. Unpublished Master Thesis. (Instituto Superior Técnico, Universidade Técnica de Lisboa: Lisboa, Portugal)

Sousa AMO, Pereira JMC, Silva JMN (2003) Evaluating the performance of multitemporal image compositing algorithms for burned area analysis. *International Journal of Remote Sensing* **24**(6), 1219–1236.

Stroppiana D, Pinnock S, Pereira JMC, Grégoire J-M (2002) Radiometric analysis of SPOT-VEGETATION images for burnt area detection in Northern Australia. *Remote Sensing of Environment* **82**, 21–37.

Swain PH (1978) Fundamentals of pattern recognition in remote sensing. In 'Remote Sensing, the Quantitative Approach'. (Eds PH Swain and SM Davis) pp.136–226. (McGraw-Hill: New York, NY)

Trigg S, Flasse S (2000) Characterizing the spectral-temporal response of burned savannah using in situ spectroradiometry and infrared thermometry. *International Journal of Remote Sensing* **21**, 3161–3168.

Tucker CJ (1996) History of the use of AVHRR data for land applications. In 'Advances in the Use of NOAA-AVHRR Data for Land Applications'. (Eds G D'Souza, AS Belward, and J-P Malingreau) pp. 1–19. (Kluwer Academic Publishers: The Netherlands)

van Wilgen BW, Scholes RJ (1997) The vegetation and fire regimes of southern-hemisphere Africa. In 'Fire in southern African savannas: ecological and atmospheric perspectives'. (Eds BW van Wilgen, MO Andreae, JG Goldammer and JA Lindesay) pp. 27–46. (Witwatersrand University Press: Johannesburg)

Verhoef W (1984) Light scattering by leaf layers with application to canopy reflectance modeling: the SAIL model. *Remote Sensing of Environment* **16**, 125–141.

Ward DE (2001) Combustion chemistry and smoke. In 'Forest fires—behavior and ecological effects'. (Eds EA Johnson and K Miyanishi) pp. 55–77. (Academic Press: San Diego)

Ward DE, Hao W-M, Susott RA, Babitt RE, Shea RW, Kaufman JB, Justice CO (1996) Effect of fuel composition on combustion efficiency and emission factors for African savanna ecosystems. *Journal of Geophysical Research* **101**, 23 569–23 576.

White F (Ed.) (1983) The vegetation of Africa. A descriptive memoir to accompany the UNESCO/AETFAT/UNSO vegetation map of Africa. (UNESCO: Paris)

Williams RJ, Griffiths AD, Allan GE (2002) Fire regimes and biodiversity in the savannas of northern Australia. In 'Flammable Australia—the fire regimes and biodiversity of a continent'. (Eds RA Bradstock, JE Williams and AM Gill) pp. 281–304. (Cambridge University Press: Cambridge, UK)

World Meteorological Organization (1994) WMO statement on the status of the global climate in 1993. WMO Report No. 809. (WMO: Geneva)